Research Article

Enhancing Disturbance Rejection of PID Controllers for DC Joint Motors of Trajectory Tracking Robots Using Disturbance Observer

Pinit Ngamsom*
Department of Mechanical Engineering, Rangsit University, Pathum Thani, Thailand

* Corresponding author. E-mail: ngamsomp@hotmail.com DOI: 10.14416/j.asep.2023.02.003
Received: 18 October 2022; Revised: 15 December 2022; Accepted: 6 January 2023; Published online: 2 February 2023

Abstract
In this paper, disturbance rejection of DC motor PID trajectory control systems is enhanced for independent joint control of robot arms. The concept of disturbance observer is invoked to propose a linear auxiliary control that augments existing PID controllers. The design of the auxiliary control is developed using a state space approach rather than transfer function approaches commonly employed in many existing designs derived from the concept of disturbance observer. This provides new insight and leads to a compact design requiring only two design parameters. While many of the existing DC motor trajectory control systems assume the availability of current feedback from a motor coil, the proposed auxiliary control does not. This can highly facilitate its applications in the lacking situation. Realizing that the stability of the resulting control systems could be inconvenient to assert due to increased system dimension resulting from incorporating disturbance observer, compact criteria for asserting robust stability using readily available results is given explicitly. To evaluate the capability of the auxiliary control for disturbance rejection, experimental results on a DC joint motor of an articulated robot arm are given. In presence of smooth and abrupt loading variations due to gravity, it appears that the tracking error of the enhanced system can be approximately 67% of that of the unenhanced system. This result is consistent in all three rounds of experiments.

Keywords: Disturbance, Rejection, Trajectory, Control, Linear, Motor, DC, PID

1 Introduction

When chosen appropriately, a robot could simultaneously deliver speed, flexibility, precision, repeatability, and safety for many tasks at an economical cost [1]–[3]. It is evident from the literature that the use of robots has increased significantly in recent years. In particular, articulated robot arms have been widely employed for tasks that require trajectory tracking capability, such as welding and paint spraying. This is primarily due to their structure, which allows a satisfactory level of dexterity for various demanding applications. However, the structure also dictates that their revolute joints are normally subjected to significant loading variation due to gravity. When an articulated robot arm handles fixed loads along fixed trajectories, the corresponding joint tracking errors are usually small because accurate compensation for the variation could be pre-computed. When operations concern with uncertainty, such compensation is not possible and the corresponding joint motor controllers have to rely on feedback signals only. In this situation, the controllers should be able to reject disturbance effectively, or tracking errors could grow significantly. For articulated robot arms, this particularly important property can be delivered by various types of controllers with varying degrees of success. A time-tested standard type for independent joint control is PID control [4]. Advanced robust control techniques, such as sliding-mode control and adaptive control have been applied to this problem in many researches [5], [6]. It has been shown that intelligent control techniques, with fuzzy logic and neural networks in particular [7], [8], could yield successful results for this application. Among many

choices of available control techniques, PID controls are advantageous in that they can be designed systematically by using well-established classical control theory. Its records of successful applications, tuning techniques, and known theoretical and practical results are abundant. Because of these, PID controls are widely adopted in many industrial applications even in the present day. These include industrial trajectory tracking robots.

Disturbance observer is a controller design technique primarily developed to deal with the problem of disturbance rejection. The original concept was proposed in Ohishi *et al.*, 1983 [9] to estimate loading torque applied to a DC motor speed control system, allowing rapid compensation accordingly. This technique is advantageous in that it allows separation of controller design for nominal systems, and disturbance rejection. In addition, it is sufficient to use simple smooth linear control laws for both. This desirable characteristic usually allows a convenient conclusion of stability using numerous existing analytical results. It has been investigated, extended, and applied in various fashions to produce successful results. A review paper [10] summarizes comprehensive development and many satisfactory applications of disturbance observer for over the last three decades. Emre and Kouhei, 2015 [11] proposed useful design guidelines that concern stability and robustness of DC motor control systems with disturbance observer.

While disturbance observer has been successfully employed in several applications of DC motor controls as mentioned previously, many are derived by using transfer function approaches. In addition, they assume availability of current feedback from motor coil, which may not be readily available or very inconvenient to obtain in some practical situations. In this study, a design of disturbance observer for DC motor trajectory control is differently proposed by using a state-space approach. This provides new insights and leads to a new compact design technique. For this, availability of current feedback from motor coil is not assumed. This allows applications of the proposed technique in situations where existing techniques do not. This paper considers a practical industrial situation in which a DC motor is employed to drive a robot joint for trajectory tracking using a PID controller. It proposes a technique for suppressing tracking error due to loading variation by augmenting a linear auxiliary controller to the existing PID controller. The auxiliary controller is derived from the concept of a disturbance observer. The proposed controller operates solely on motor shaft angular position and speed feedback signals. Neither pre-computed loading torque nor current feedback is required. A convenient condition for guaranteed input-to-state stability is given. Performance of the auxiliary controller is evaluated by performing experiments on a joint motor of an articulated robot arm. When the motor is subjected to smooth and abrupt loading variation, it appears consistently in experiments that the auxiliary controller can reduce the tracking error of an existing PID control system significantly.

2 Mathematical Model of DC Motors with Mechanical Transmission

Brushed DC motors are electromechanical devices employed to drive the joints of many small and medium-sized robots. They possess desirable characteristics of being economical and simple to drive. They give a good level of torque, which is required to achieve high angular acceleration and performance of robot joints. However, their mechanical commutation produces brush wear and requires periodic maintenance. Electronic commutation is employed in a 3-phase brushless DC motor to eliminate the use of mechanical brushes. The fact that such commutation can produce significant torque ripple is long known [12]. This undesirable characteristic could be considerably suppressed by using specialized modern electronic drives, such as ODrive, although the associated cost could be more than that of the motor. Details of commutation is not discussed in here, and ideal commutation is assumed in the rest of the discussion.

Although a mathematical model of DC motors with mechanical transmission is a topic that can be found in many works of literature on dynamic systems and control, it is discussed briefly in this section so that critical meanings of parameters and terms can be made certain. Consider the schematic diagram of a DC motor with mechanical transmission depicted in Figure 1. All the notations associated with it are given in Table 1. Typically, the parameters J_m, b_m, and b_L are regarded as constants, while J_L can increase considerably when the robot handles heavy objects.

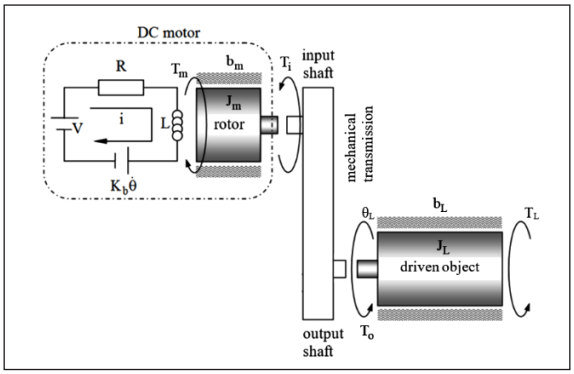

Figure 1: Schematic diagram of a typical joint motor with mechanical transmission.

Table 1: Parameters, torques, and variables associated with a DC joint motor and mechanical transmission

Symbol	Meaning (unit)
J_m	mass moment of inertia of rotor about rotational axis (kg.m^2)
J_L	mass moment of inertia of driven object about rotational axis (kg.m^2)
J	effective mass moment of inertia (kg.m^2)
b_m	coefficients of viscous friction of rotor (N.m.s/rad)
b_L	coefficients of viscous friction of object (N.m.s/rad)
b	effective coefficients of viscous friction (N.m.s/rad)
K_T	motor torque constant (N.m/A)
K_b	back-EMF constant (V.s/rad)
R	coil resistance (Ohm)
L	coil inductance (Henry)
T_m	motor torque generated by electrical current in motor coils (N.m)
T_L	loading torque applied to the driven object (N.m)
T_i	torque exerted to the rotor by transmission input shaft (N.m)
T_o	torque exerted to the driven object by transmission output shaft (N.m)
T_d	effective loading torque (N.m)
V	input voltage to motor coil (V)
θ	angular displacement of the rotor (rad)
θ_L	angular displacement of the driven object (rad)
i	electrical current in motor coil (A)
r_T	transmission ratio
η_g	transmission efficiency

According to Figure 1, Newton-Euler moment equations can be written as [13]:

$$T_m - T_i - b_m\dot{\theta} = J_m\ddot{\theta} \tag{1}$$

$$T_o + T_L - b_L\dot{\theta}_L = J_L\ddot{\theta}_L \tag{2}$$

where θ and θ_L are the angular displacement of the rotor and the driven object, respectively. Note that Equations (1) and (2) are for the rotor and the driven object respectively.

Mechanical energy transmission from rotor to driven object is described by:

$$\eta_g T_i\theta = T_o\theta_L \tag{3}$$

where η_g is the transmission efficiency. Equation (3) can be written as:

$$\eta_g T_i\left(\frac{\theta}{\theta_L}\right) = T_o \tag{4}$$

where $r_T \equiv \theta/\theta_L$ is the transmission ratio. For robots, Equation (4) is normally written so that $r_T > 1$ for torque amplification. It follows that $\theta = r_T\theta_L$, implying that $\dot{\theta} = r_T\dot{\theta}_L$ and that $\ddot{\theta} = r_T\ddot{\theta}_L$. From these equations, it can be shown that:

$$\underbrace{\left(J_m + \frac{J_L}{\eta_g r_T^2}\right)}_{J}\ddot{\theta} - \underbrace{\left(b_m + \frac{b_L}{\eta_g r_T^2}\right)}_{b}\dot{\theta} = T_m + \underbrace{\left(\frac{T_L}{\eta_g r_T}\right)}_{T_d}$$

Because the motor torque T_m is proportional to the electrical current i in motor coils, it follows that $T_m = K_T i$ where K_T is torque constant of the motor. Substitute this in the above equation to obtain:

$$J\ddot{\theta} + b\dot{\theta} = K_T i + T_d \tag{5}$$

where $J \equiv J_m + J_L/(\eta_g r_T^2)$ is the effective mass moment of inertia of the motor-transmission system, $b \equiv b_m + b_L/(\eta_g r_T^2)$ is the effective coefficient of viscous friction, and $T_d \equiv T_L/(\eta_g r_T)$ is the effective loading torque. During robot operations, there can be variations of J_L, or T_L, or both can vary simultaneously. These change the values of J and T_d, and usually yield undesirable consequences for the control system. To alleviate these, typical robot joints could use a transmission ratio r_T that is significantly larger than J_L and the ratio $J_L/(\eta_g r_T^2)$ is much smaller than J_m. With this, variation of J_L affects the value of J so slightly that J can usually be regarded as a constant. Because $T_d \equiv T_L/(\eta_g r_T)$, effects of T_L on T_d can be attenuated considerably by using a large value for r_T. Notice that

the attenuation on T_L is due to r_T while that on J_L is due to r_T^2. Accordingly, the degree of attenuation on T_L is much weaker than the other. This paper discusses a typical situation in which variation of J_L about its nominal value is small and r_T is fairly large, making it reasonable to neglect variation of J. Given this, it is desirable to attenuate effects of T_d on tracking error. Note that the Coulomb friction moment about the rotation axes of the rotor and the driven object may be considered a part of T_d for convenience.

In Figure 1, motor electrical parameters are coil inductance L, coil resistance R, and back-EMF constant K_b. Kirchhoff's voltage law [13] is applied to the circuit of motor coil to obtain:

$$L\left(\frac{di}{dt}\right)+iR+K_b\dot{\theta}=V \tag{6}$$

where V is the input voltage to motor coil. Typically, dynamics of the coil current i is much faster than that of the angular displacement θ of the rotor. This can be shown mathematically by obtaining the Laplace transform of θ from Equations (5) and (6), and making use of the fact that the values of J, L, and b are typically much smaller than that of the remaining parameters. With this, dynamics of θ in Equations (5) and (6) can be approximated by the following reduced-order model:

$$\ddot{\theta}=-\left(\frac{K_TK_b}{JR}+\frac{b}{J}\right)\dot{\theta}+\left(\frac{K_T}{JR}\right)V+\left(\frac{1}{J}\right)T_d \tag{7}$$

Typically, Bode plots of transfer functions $\theta(s)/V(s)$ and $\theta(s)/T_d(s)$ from Equations (5) and (6) and those from Equation (7) are almost identical when frequencies of $V(t)$ and $T_d(t)$ do not exceed 1 kHz. Electronic hardwares of many trajectory tracking robots are such that $V(t)$ obeys this frequency bound. The frequency of $T_d(t)$ is typically much lower than that. These justify the use of Equation (7) to approximate Equations (5) and (6) in this frequency range. Note that some robot control systems may not have a sensor and relevant electronic circuitry for measuring i. In this situation, it is convenient to use Equation (7) rather than Equations (5) and (6) for the proposed controller design.

3 Controller Design

By assumption, the values of all parameters can be reasonably regarded as constants. They can be determined accurately by using appropriate setup and modern precision measuring instruments. This is not the case for T_d, which can vary significantly in various fashions, and its value is generally unknown to the controller. However, a joint motor controller should be designed specifically to handle this, or tracking error could grow unacceptably.

Now define state variables $q_1 \equiv \int \theta\, dt$, $q_2 \equiv \theta$, $q_3 \equiv \dot{\theta}$, and state vector $q \equiv [q_1\ q_2\ q_3]^T$. These state equations and Equation (7) can be written in vector-matrix form as:

$$\underbrace{\begin{bmatrix}\dot{q}_1\\ \dot{q}_2\\ \dot{q}_3\end{bmatrix}}_{\dot{q}}=\underbrace{\left[\begin{array}{c|c|c}0&1&0\\ \hline 0&0&1\\ \hline 0&0&-\left(\frac{K_TK_b}{JR}+\frac{b}{J}\right)\end{array}\right]}_{A}\underbrace{\begin{bmatrix}q_1\\ q_2\\ q_3\end{bmatrix}}_{q}+\underbrace{\begin{bmatrix}0\\ 0\\ \frac{K_T}{JR}\end{bmatrix}}_{B}u+\underbrace{\begin{bmatrix}0\\ 0\\ \frac{1}{J}\end{bmatrix}}_{N}T_d$$

or

$$\dot{\boldsymbol{q}}=\boldsymbol{A}\boldsymbol{q}+\boldsymbol{B}u+\boldsymbol{N}T_d \tag{8}$$

where the control input u is the input voltage V. Accurate value of θ must be available for feedback at all times. This allows us to determine $\int \theta\, dt$ very accurately. Theoretically, θ cannot be used to determine $\dot{\theta}$ very accurately. Because of this, it is usually required that $\dot{\theta}$ is available for feedback when satisfying performance is expected. Let θ_r be the reference trajectory for the joint angle θ. Now, define $r_1 \equiv \int \theta_r\, dt$, $r_2 \equiv \theta_r$, $r_3 \equiv \dot{\theta}_r$, and $\boldsymbol{r} \equiv [r_1\ r_2\ r_3]^T$. Because the reference trajectory θ_r is known prior to operating the robot, it follows that the reference vector $\boldsymbol{r}$ is known. Accordingly, the error vector is obtained as $\boldsymbol{e} \equiv \boldsymbol{r} - \boldsymbol{q} \equiv [e_1\ e_2\ e_3]^T$.

The resultant control input u is composed of two components:

$$u = u_n + u_a \tag{9}$$

where $u_n = -\boldsymbol{K}\boldsymbol{e}$ is the nominal PID control, $\boldsymbol{K} = [k_1\ k_2\ k_3] \in \Re^3$, and u_a is the auxiliary control to obtain. The former component is to stabilize the system with acceptable performance, while the latter component is to attenuate effects of T_d. Substitute $u = u_n + u_a$, $\boldsymbol{q} = \boldsymbol{r} - \boldsymbol{e}$, and $\dot{\boldsymbol{q}} = \dot{\boldsymbol{r}} - \dot{\boldsymbol{e}}$ in Equation (8) and manipulate terms to obtain the following equation:

$$\dot{\boldsymbol{e}} = \boldsymbol{A}\boldsymbol{e} + \bar{\boldsymbol{B}}u + \bar{\boldsymbol{r}} + \bar{\boldsymbol{N}}T_d \tag{10}$$

where $\bar{\boldsymbol{B}} \equiv -\boldsymbol{B}$, $\bar{\boldsymbol{N}} \equiv -\boldsymbol{N}$, and $\bar{\boldsymbol{r}} \equiv -\boldsymbol{A}\boldsymbol{r} + \dot{\boldsymbol{r}}$. Here, the nominal PID control u_n is to be designed or is readily available prior to design the auxiliary control u_a. Disturbance rejection of the nominal control system need not be very satisfactory because it could be improved by augmenting the auxiliary control. A design technique for the nominal control is not discussed in here because there already are several existing techniques, which can be employed to produce satisfying results. Although the two control components are designed separately, the resultant control u must be able to guarantee the stability of the resulting control system.

To obtain the auxiliary control, denote the elements $\boldsymbol{A}(3,3)$, $\bar{\boldsymbol{B}}(3,1)$, and $\bar{\boldsymbol{N}}(3,1)$ by a, $\bar{b}$, and $\bar{n}$ respectively. Notice that the structures of $\bar{\boldsymbol{B}}$ and $\bar{\boldsymbol{N}}$ indicate that u and T_d have direct effects on $\dot{e}_3$. Extract $\dot{e}_3$ from Equation (10), and manipulate terms to obtain that:

$$\dot{e}_3 - ae_3 - \bar{b}u_n = \bar{b}u_a + \underbrace{\bar{n}T_d - ar_3 + \dot{r}_3}_{T_\Sigma} \tag{11}$$

The term T_Σ in the right-hand side of Equation (11) could be considered as the total disturbance resulting from the loading torque T_d, and time-varying nature of the reference trajectory θ_r. If this term is absent, the result is an ideal linear dynamical system, for which existing controller design techniques could be employed to obtain a nominal control that delivers very satisfactory results. In this paper, the concept of disturbance observer is employed to derive an auxiliary control u_a for suppressing T_Σ. By direct observation, it could be seen from Equation (11) that a possible choice of u_a for this purpose is:

$$u_a = -\frac{\gamma}{\bar{b}_n}(\dot{e}_{3f} - a_n e_3 - \bar{b}_n u_n) \tag{12}$$

where a_n is a nominal value of a, $\bar{b}_n$ is a nominal value of $\bar{b}$, γ is a design parameter that governs strength of suppression on the total disturbance, $\dot{e}_{3f} = \ddot{\theta}_r - \ddot{\theta}_f$, $\ddot{\theta}_r$ is the second time derivative of the reference trajectory θ_r, and $\ddot{\theta}_f$ is an approximation of $\ddot{\theta}$. Because the reference trajectory θ_r is known before operating the robot, $\ddot{\theta}_r$ can be computed accordingly. Depending on how accurately $\bar{b}_n$ approximates $\bar{b} \equiv -K_T/(JR)$, it is recommended that $0 < \gamma \leq 1$. When the accuracy is low, accurate disturbance compensation should not be expected in the beginning. In this situation, a small value of γ should be selected. It can be increased when satisfactory disturbance rejection is observed from system responses. Note that $\ddot{\theta}_f$ is employed rather than $\ddot{\theta}$ because the angular acceleration $\ddot{\theta}$ is not available for feedback. It is elected that $\ddot{\theta}_f$ is the output of a Low-Pass Differentiator (LPD) whose input is the angular velocity $\dot{\theta} \equiv q_3$ of the rotor. The LPD is simply a cascading combination of a differentiator and a low-pass filter. The reason for using a differentiator is obvious, while the reason for using a low-pass filter is because differentiation of the velocity is usually very sensitive to noises. A second-order filter with two repeated poles is elected for this. Note that y_f is now employed to denote the output of the LPD to avoid confusion of similar symbols, and the following transfer function is proposed for the LPD:

$$\frac{Y_f(s)}{Q_3(s)} = \frac{a_f^2 s}{(s + a_f)^2}$$

where $y_f(s)$ and $Q_3(s)$ are Laplace transform of y_f and q_3 respectively. The parameter $a_f \in \Re^+$ determines the cut-off frequency of the filter, which must be greater than zero for the stability of the filter. It should be slightly higher than the frequency of the load torque to obtain valid filter output while suppressing noises. Because $\ddot{\theta}$ is immediately affected by variation of T_d, the value of this parameter should be higher than the highest expected frequency of T_d and smaller than the lowest frequency of expected noises. It can be shown that a state-space representation of the LPD is given by:

$$\begin{bmatrix} \dot{w}_1 \\ \dot{w}_2 \end{bmatrix} = \begin{bmatrix} 0 & 1 \\ -a_f^2 & -2a_f \end{bmatrix} \begin{bmatrix} w_1 \\ w_2 \end{bmatrix} + \begin{bmatrix} 0 \\ 1 \end{bmatrix} q_3 \tag{13}$$

$$y_f = \begin{bmatrix} 0 & a_f^2 \end{bmatrix} \begin{bmatrix} w_1 \\ w_2 \end{bmatrix} \tag{14}$$

where w_1 and w_2 are state variables of the LPD.

Structure of the proposed control system is shown in Figure 2. The signals θ and $\dot{\theta}$ are drawn from the joint motor assembly. Next, $\theta \equiv q_2$ and $\dot{\theta} \equiv q_3$ are fed to an integrator and the LPD respectively to obtain the signals $\int \theta\, dt \equiv q_1$ and $\ddot{\theta}_f$. The nominal PID controller takes $[q_1, q_2, q_3]$ and $[\int \theta_r\, dt, \theta_r, \dot{\theta}_r]$ to produce

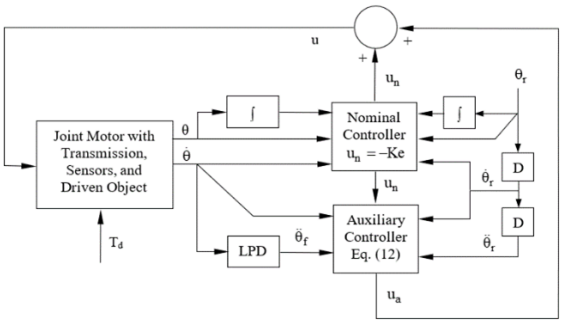

Figure 2: Schematic diagram of the proposed control system.

the nominal control $u_n = -\boldsymbol{Ke}$. The auxiliary controller employs u_n, $\dot{\theta}$, $\dot{\theta}_r$, $\ddot{\theta}_f$, and $\ddot{\theta}_r$ in accordance with Equation (12) to produce the auxiliary control u_a. Finally, the resultant control $u = u_n + u_a$ can be obtained.

The resultant control can be written in a compact form, which is convenient for real implementation. For this, recall from Equation (9) that $u = u_n + u_a$. Now, substitute for u_a using Equation (12), and substitute $u_n = -\boldsymbol{Ke}$ to produce:

$$u = -\boldsymbol{Ke} - \frac{\gamma}{b_n}\dot{e}_{3f} + \gamma\frac{a_n}{b_n}e_3 - \gamma\boldsymbol{Ke}$$

By substituting $\boldsymbol{K} = [k_1\ k_2\ k_3]$ in the above equation and manipulating terms, it can be shown that:

$$u = -\underbrace{\left[c_1k_1 \mid c_1k_2 \mid c_1k_3 - c_2 \mid c_3\right]}_{\boldsymbol{K}_f}\underbrace{\left[e_1\ \ e_2\ \ e_3\ \ \dot{e}_{3f}\right]^T}_{\boldsymbol{e}_f} \tag{15}$$

where $\boldsymbol{K}_f \equiv \left[c_1k_1 \mid c_1k_2 \mid c_1k_3 - c_2 \mid c_3\right] \equiv \left[k_{f1}\ k_{f2}\ k_{f3}\ k_{f4}\right]$,

$c_1 \equiv (1+\gamma), c_2 \equiv \gamma(a_n/\bar{b}_n), c_3 \equiv \gamma/\bar{b}_n$, and $\boldsymbol{e}_f \equiv \left[e_1\ e_2\ e_3\ \dot{e}_{3f}\right]^T$.

4 Stability Analysis

Recall that Equation (7) approximates the dynamics of the DC joint motor in Equations (5) and (6) very well, and allows convenience of designing controllers without using i as a feedback signal. However, Equations (5) and (6) are employed for analyzing the stability of the resulting control system in this section because of crucial importance of stability in any control system.

Recalling state variables $q_1 \equiv \int \theta\, dt$, $q_2 \equiv \theta$, and $q_3 \equiv \dot{\theta}$ defined previously, now define an additional state variable $q_4 \equiv i$. These state equations may be written with Equations (5) and (6) in vector-matrix form as:

$$\begin{bmatrix}\dot{q}_1\\ \dot{q}_2\\ \dot{q}_3\\ \dot{q}_4\end{bmatrix} = \left[\begin{array}{c|c|c|c} 0 & 1 & 0 & 0\\ \hline 0 & 0 & 1 & 0\\ \hline 0 & 0 & -\frac{b}{J} & \frac{K_T}{J}\\ \hline 0 & 0 & -\frac{K_b}{L} & -\frac{R}{L}\end{array}\right]\begin{bmatrix}q_1\\ q_2\\ q_3\\ q_4\end{bmatrix} + \begin{bmatrix}0\\ 0\\ 0\\ \frac{1}{L}\end{bmatrix}V + \begin{bmatrix}0\\ 0\\ \frac{1}{J}\\ 0\end{bmatrix}T_d \tag{16}$$

Dynamics of the LPD in Equations (13) and (14) can be augmented to Equation (16) to produce:

$$\underbrace{\begin{bmatrix}\dot{q}_1\\ \dot{q}_2\\ \dot{q}_3\\ \dot{q}_4\\ \dot{w}_1\\ \dot{w}_2\end{bmatrix}}_{\dot{\boldsymbol{q}}_w} = \underbrace{\left[\begin{array}{cccc|cc} 0 & 1 & 0 & 0 & 0 & 0\\ 0 & 0 & 1 & 0 & 0 & 0\\ 0 & 0 & -\frac{b}{J} & \frac{K_T}{J} & 0 & 0\\ 0 & 0 & -\frac{K_b}{L} & -\frac{R}{L} & 0 & 0\\ \hline 0 & 0 & 0 & 0 & 0 & 1\\ 0 & 0 & 1 & 0 & -a_f^2 & -2a_f\end{array}\right]}_{\boldsymbol{A}_w}\underbrace{\begin{bmatrix}q_1\\ q_2\\ q_3\\ q_4\\ w_1\\ w_2\end{bmatrix}}_{\boldsymbol{q}_w} + \underbrace{\begin{bmatrix}0\\ 0\\ 0\\ \frac{1}{L}\\ 0\\ 0\end{bmatrix}}_{\boldsymbol{B}_w}u + \underbrace{\begin{bmatrix}0 & 0 & \frac{1}{J} & 0 & 0 & 0\end{bmatrix}^T}_{\boldsymbol{N}_w}T_d$$

and

$$\left[y_f\right] = \left[\begin{array}{cccc|cc} 0 & 0 & 0 & 0 & 0 & a_f^2\end{array}\right]\left[q_1\ \ q_2\ \ q_3\ \ q_4 \mid w_1\ \ w_2\right]^T$$

For later development, write the above state equation in a compact form:

$$\dot{\boldsymbol{q}}_w = \boldsymbol{A}_w\boldsymbol{q}_w + \boldsymbol{B}_w u + \boldsymbol{N}_w T_d \tag{17}$$

The dimension of the state-space system in Equation (17) is six. For stability analysis, it is desirable to rewrite the resultant control $u \equiv -\boldsymbol{K}_f\boldsymbol{e}_f$ in Equation (15) to accommodate this. Recall from the previous section that:

$$u = -\left[k_{f1}\ \ k_{f2}\ \ k_{f3}\ \ k_{f4}\right]\left[e_1\ \ e_2\ \ e_3\ \ \dot{e}_{3f}\right]^T$$

where it has been defined that $\dot{e}_{3f} \equiv \ddot{\theta}_r - \ddot{\theta}_f$, and $\ddot{\theta}_f \equiv y_f$.

For compact representation, denote $\ddot{\theta}_r \equiv r_4$. With this, the last equation can be written as:

$$u = \left[k_{f1} \mid k_{f2} \mid k_{f3} \mid k_{f4}\right]\left[q_1 \mid q_2 \mid q_3 \mid y_f\right]^T - \left[k_{f1} \mid k_{f2} \mid k_{f3} \mid k_{f4}\right]\left[r_1 \mid r_2 \mid r_3 \mid r_4\right]^T$$

Now, substitute $y_f = a_f^2 w_2$ from Equation (14) in the above equation. With some vector manipulation, it can be shown that:

$$u = \underbrace{\left[k_{f1} \;\; k_{f2} \;\; k_{f3} \;\; 0 \mid 0 \;\; k_{f4}a_f^2\right]}_{\boldsymbol{K}_w}\underbrace{\left[q_1 \;\; q_2 \;\; q_3 \;\; q_4 \mid w_1 \;\; w_2\right]^T}_{\boldsymbol{q}_w} - \underbrace{\left[k_{f1} \mid k_{f2} \mid k_{f3} \mid k_{f4}\right]}_{\boldsymbol{K}_f}\underbrace{\left[r_1 \mid r_2 \mid r_3 \mid r_4\right]^T}_{\boldsymbol{r}_f}$$

Finally, it can be shown that:

$$u = \boldsymbol{K}_w\boldsymbol{q}_w - \boldsymbol{K}_f\boldsymbol{r}_f \tag{18}$$

where $\boldsymbol{K}_w \equiv \left[k_{f1} \;\; k_{f2} \;\; k_{f3} \;\; 0 \mid 0 \;\; k_{f4}a_f^2\right]$, $\boldsymbol{q}_w \equiv \left[q_1 \;\; q_2 \;\; q_3 \;\; q_4 \mid w_1 \;\; w_2\right]^T$ and $\boldsymbol{r}_f \equiv \left[r_1 \mid r_2 \mid r_3 \mid r_4\right]^T$.

To obtain error dynamics corresponding to the system in Equation (17), define $\boldsymbol{r}_w \equiv \left[r_1 \;\; r_2 \;\; r_3 \;\; r_4 \;\; 0 \;\; 0\right]^T$, and $\boldsymbol{e}_w \equiv \boldsymbol{r}_w - \boldsymbol{q}_w$. Substitute $\boldsymbol{q}_w = \boldsymbol{r}_w - \boldsymbol{e}_w$, $\dot{\boldsymbol{q}}_w = \dot{\boldsymbol{r}}_w - \dot{\boldsymbol{e}}_w$, and $u = \boldsymbol{K}_w\boldsymbol{q}_w - \boldsymbol{K}_f\boldsymbol{r}_f$ from Equation (18) in Equation (17) to obtain:

$$\dot{\boldsymbol{e}}_w = \underbrace{(\boldsymbol{A}_w + \boldsymbol{B}_w\boldsymbol{K}_w)}_{\tilde{\boldsymbol{A}}_w}\boldsymbol{e}_w + \boldsymbol{p}(t) \tag{19}$$

where $\boldsymbol{p}(t) \equiv \dot{\boldsymbol{r}}_w - \tilde{\boldsymbol{A}}_w\boldsymbol{r}_w + \boldsymbol{B}_w\boldsymbol{K}_f\boldsymbol{r}_f - \boldsymbol{N}_wT_d$ and $\tilde{\boldsymbol{A}}_w \equiv \boldsymbol{A}_w + \boldsymbol{B}_w\boldsymbol{K}_w$. Note also that $\boldsymbol{p}(t)$ is a bounded perturbation vector that does not depend on $\boldsymbol{e}_w$. The error dynamics of Equation (19) is in a form that can be employed to assert input-to-state stability of the control system using existing results. This type of stability guarantees that all trajectories of the system converge to a neighborhood about the origin when $\boldsymbol{p}(t) \neq 0$, and the extent of this neighborhood increases as the magnitude of $\boldsymbol{p}(t)$ increases. Clearly, this is a reasonable condition for the application of interest. It can be shown that input-to-state stability is guaranteed when the origin of the system in Equation (19) is uniformly globally exponentially stable [14]. In the case of interest, $\tilde{\boldsymbol{A}}_w$ is a constant matrix. Accordingly, this is equivalent to the condition that $\tilde{\boldsymbol{A}}_w$ is strictly Hurwitz.

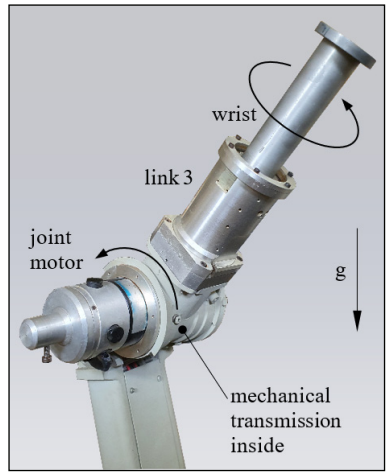

Figure 3: Joint motor and links of the articulated robot arm in the experiments.

All the motor parameters determined in practice are associated with some degrees of error. However, the robustness of the control system to parameter uncertainty is not discussed extensively here because the present aspect of interest is disturbance rejection. Theoretically, the condition that $\tilde{\boldsymbol{A}}_w$ is strictly Hurwitz guarantees that the system is input-to-state stable when values of all the parameters are sufficiently accurate. If accurate values of some parameters are not available, then their upper and lower bounds should be determined. Using these bounds, existing robust stability analysis theorems can guarantee that the control system is robustly stable for all possible values of the parameters within such bounds. For readers particularly interested in robust stability of linear systems, such theorems can be found in [15]–[17].

5 Experimental Results

In this section, the design of the proposed auxiliary control and stability analysis of the resulting trajectory-tracking DC motor control system are shown. The motor is to drive a revolute joint of an articulated robot arm. This joint is connected to link 3 and the wrist of the robot arm as shown in Figure 3. Because the center of mass of the link and wrist assembly is not on the rotation axis of the joint, the joint motor is subjected to variation of loading torque due to gravity as shown in Figures 3 and 4. The nominal values of the relevant parameters are given in Table 2.

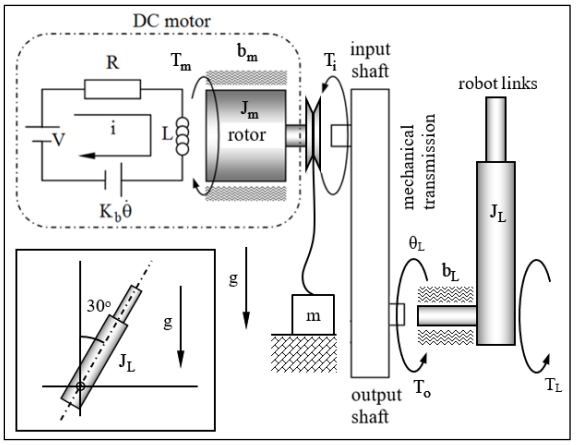

Figure 4: A setup for introducing abrupt loading torque to the joint motor.

Table 2: Values of parameters of DC joint motor with mechanical transmission in Equations (5) and (6)

Symbol	Meaning (value)
J	effective mass moment of inertia (0.00017 kg.m^2)
b	effective coefficients of viscous friction (0.0023 N.m.s/rad)
K_T	motor torque constant (0.185 N.m/A)
K_b	back-EMF constant (0.185 V.s/rad)
R	coil resistance (5.2 Ω)
L	coil inductance (2.0 mH)

Note that values of parameters R, and L are directly measured by a precision instrument. The others are obtained indirectly from experiments on the actual joint motor of the robot. Substituting these values in the mathematical model of Equations (5) –(7), it can be verified that resulting system responses from numerical simulations are very similar to corresponding actual system responses. These hold for step and sinusoidal inputs of different magnitudes, indicating that the values are valid estimations of the respective parameters. The joint of interest employs a mechanical transmission ratio of $r_T = 100$. The angular displacement of the joint motor shaft is measured by an incremental encoder and a decoding circuit, giving 2048 pulses per motor shaft revolution, or 204800 pulses per joint revolution. The angular velocity of the shaft is approximated by using filtered backward differentiation of the angular displacement. This is a typical practice employed in industrial robots and research including Ohishi *et al.*, [9], and it has been experimentally verified that the approximation is valid. The sampling period of the control system is 1 ms. Consider the situation in which the joint motor is to track a reference trajectory without attaching any additional mass directly to link 3 and the wrist. In this situation, it is reasonable to treat the effective mass moment of inertia J as a constant.

Now that accurate values of all parameters are available, the reduced-order model in Equation (10) is employed to obtain the nominal PID control u_n. Note that the existing hardware of the robot has neither a sensor nor an electronic circuit for measuring current in the motor coil. No modification is made to incorporate these into the existing hardware because this is very inconvenient, expensive, and time-consuming. In addition, adopting coil current for feedback means that the control program must be modified accordingly. A nominal PID control can be obtained by using any existing techniques. Here, LQR (Linear Quadratic Regulator) theory is employed because it is a well-known technique and is capable of giving a satisfactorily large stability margin [15]. The design of a PID controller using LQR theory is not of interest to this paper, so it is briefly summarized in the following. Without the auxiliary control, $u = u_n = -\boldsymbol{Ke}$, and the corresponding performance index of the LQR is:

$$J_c = \int_0^\infty (\boldsymbol{e}^T \boldsymbol{Q} \boldsymbol{e} + u_n^T \boldsymbol{R} u_n) dt$$

where it is imposed that $\boldsymbol{Q}$ and $\boldsymbol{R}$ are diagonal and positive definite symmetric for simplicity. It appears in numerical simulations and experiments that acceptable results can be obtained by choosing $\boldsymbol{R} = [1]$ and:

$$\boldsymbol{Q} = \begin{bmatrix} 1 & 0 & 0 \\ 0 & 100 & 0 \\ 0 & 0 & 1 \end{bmatrix}$$

The corresponding nominal linear feedback gain matrix is $\boldsymbol{K} = [-1\ -10.1\ -0.83]$. The eigenvalues of $\boldsymbol{A} - \bar{\boldsymbol{B}}\boldsymbol{K}$ are $s_1 = -215.48$, $s_2 = -9.71$, and $s_3 = -0.10$. They are all in the LHP, indicating that the nominal control system is asymptotically stable.

The auxiliary control u_a is now introduced to improve the ability to reject effects of T_d. The resultant control $u = u_n + u_a$ is determined from Equation (15).

Setting $\gamma = 0.5$ to allow moderate suppression of total disturbance and $a_f = 10$ to allow compensation for T_d at reasonable frequencies, it can be shown that $u = -\boldsymbol{K}_f \boldsymbol{e}_f$ in which:

$$\boldsymbol{K}_f = \begin{bmatrix} -1.5 & -15.16 & -1.37 & -0.0024 \end{bmatrix}$$

To investigate the stability of the resulting tracking control system, Equations (18) and (19) are employed. The above resultant control corresponds to the gain matrix:

$$\boldsymbol{K}_w \equiv \left[\begin{array}{cccc|cc} -1.5 & -15.16 & -1.37 & 0 & 0 & -0.24 \end{array}\right]$$

Using definitions of matrices $\boldsymbol{A}_w$ and $\boldsymbol{B}_w$ given in Section 4, it can be shown that $\tilde{\boldsymbol{A}}_w \equiv \boldsymbol{A}_w + \boldsymbol{B}_w \boldsymbol{K}_w$ is:

$$\tilde{\boldsymbol{A}}_w = \left[\begin{array}{cccc|cc} 0 & 1 & 0 & 0 & 0 & 0 \\ 0 & 0 & 1 & 0 & 0 & 0 \\ 0 & 0 & -13.5 & 1088.2 & 0 & 0 \\ -750 & -7580.2 & -775.1 & -2600 & 0 & -119.5 \\ \hline 0 & 0 & 0 & 0 & 0 & 1 \\ 0 & 0 & 1 & 0 & -100 & -20 \end{array}\right]$$

The eigenvalues of the matrix $\tilde{\boldsymbol{A}}_w$ are $s_1 = -2219.3$, $s_2 = -384.37$, s_3, $s_4 = -8.45 \pm j1.79$, $s_5 = -12.84$, and $s_6 = -0.1$, indicating that $\tilde{\boldsymbol{A}}_w$ is strictly Hurwitz.

Accordingly, the resulting control system is input-to-state stable, provided that the values of all the parameters are sufficiently accurate and constant. This theoretical result confirms that all trajectories of the error dynamics in Equation (19) converge to a neighborhood about the origin [14]. By this, the stability of the control system is guaranteed when values of all parameters are sufficiently accurate [14]–[17]. The following experimental results support this.

Although all values of the parameters are repeatedly verified to be accurate, it is also shown in the following that the resulting control system is robustly stable to reasonably large parameter uncertainty. When compared to the rest of the parameters, note that estimating an accurate value for J is usually the most difficult. This is because a direct measuring device for this is not available. Experiments and numerical verification are needed for its estimation as mentioned. By definition of $\tilde{\boldsymbol{A}}_w \equiv \boldsymbol{A}_w + \boldsymbol{B}_w \boldsymbol{K}_w$, uncertainty of J produces uncertainty of elements $\tilde{\boldsymbol{A}}_w(3, 3)$ and $\tilde{\boldsymbol{A}}_w(3, 4)$. Now, consider the exaggerated situation in which the true values of these elements are within a band of ±10% about their nominal values of –13.5 and 1088.2 respectively. That is,

$\tilde{\boldsymbol{A}}_w(3, 3) \in [-14.88, -12.17]$,
$\tilde{\boldsymbol{A}}_w(3, 4) \in [979.38, 1197]$.

These interval uncertainties produce 4 possible values of $\tilde{\boldsymbol{A}}_w$ at their extremes. These are denoted by $\tilde{\boldsymbol{A}}_{wj}$, $j = 1,..., 4$. Their elements are the same as those of the nominal $\tilde{\boldsymbol{A}}_w$, except that $\tilde{\boldsymbol{A}}_{wj}(3, 3)$, and $\tilde{\boldsymbol{A}}_{wj}(3, 4)$ are the extremes of the two intervals. It can be shown using a quadratic Lyapunov function $V(\boldsymbol{e}_w) = \boldsymbol{e}_w^T \boldsymbol{P} \boldsymbol{e}_w$ and LMI (Linear Matrix Inequality) that the unperturbed uncertain control system is quadratically stable [17]. The MATLAB LMI toolbox gives the following positive definite real symmetric matrix $\boldsymbol{P}$:

$$\boldsymbol{P} = \begin{bmatrix} 5.93 & 1.17 & 2.31\times10^{-3} & 7.69\times10^{-4} & 7.29\times10^{-2} & 8.90\times10^{-4} \\ . & 5.56 & 5.66\times10^{-3} & 3.13\times10^{-4} & -9.97\times10^{-2} & 8.87\times10^{-3} \\ . & . & 2.22\times10^{-3} & 7.11\times10^{-4} & -2.59\times10^{-4} & -1.85\times10^{-5} \\ . & . & . & 7.21\times10^{-4} & -1.08\times10^{-4} & -4.01\times10^{-5} \\ . & . & . & . & 5.35 & 1.14\times10^{-2} \\ . & . & . & . & . & 5.28\times10^{-2} \end{bmatrix}$$

Note that all the eigenvalues of $\tilde{\boldsymbol{A}}_{wj}^T \boldsymbol{P} + \boldsymbol{P} \tilde{\boldsymbol{A}}_{wj}$ are negative real for all j. It can be shown that the resulting control system can tolerate additional uncertainty. However, robustness is not of primary interest to the paper and will not be discussed further.

Experiments are now conducted to investigate how well the auxiliary control can reject smooth and abrupt changes in loading torque about the motor shaft. Smooth loading variation is due to the weight of link 3 and wrist assembly. This is attenuated by the use of mechanical transmission before entering the motor. Abrupt loading torque is introduced directly to the motor without attenuation. For this, a pulley of radius $r_m = 14$ mm is mounted to the shaft, and a string is attached to the pulley. The other end of the string is tied to a steel disk of mass $m = 0.73$ kg, which is placed on the floor. The string is set such that the disk is pulled up in the air and dropped down to the floor at certain points along the reference trajectory $\theta_r(t) = 4\ sin(t)$ revolution of the motor. Figure 4 depicts this setup. In all of the experiments, the initial angle between the vertical line and the center line of link 3

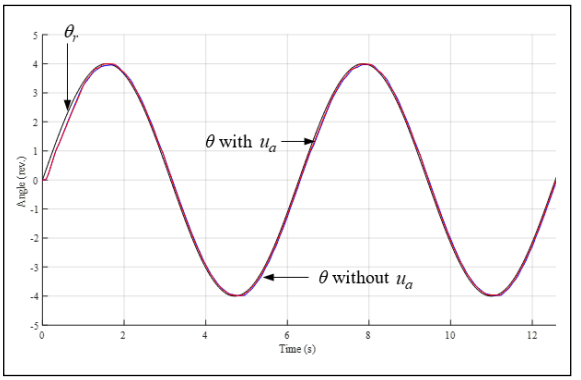

Figure 5: Reference and actual trajectories of the motor, with and without auxiliary control (unit: revolution).

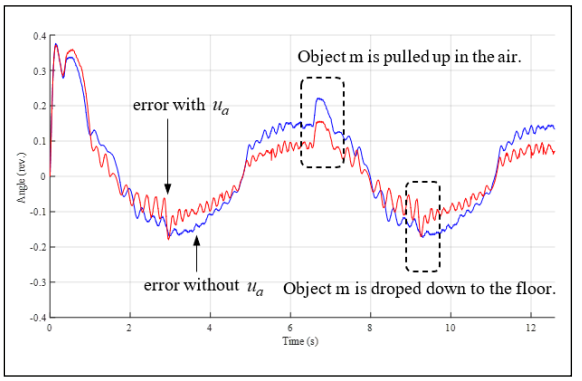

Figure 6: Tracking errors with and without auxiliary control (unit: revolution).

and the wrist is 30 degrees as shown in Figure 4. At this configuration, it is imposed that the initial state vector $\boldsymbol{q}_w(0) = \mathbf{0}$.

The experimental results are shown in Figures 5–7. Figure 5 shows the reference trajectory of the motor, the actual trajectory with auxiliary control, and the actual trajectory without auxiliary control. The two actual trajectories track the reference trajectory very closely that it is hard to distinguish one from the others after approximately 1.5 s. Figure 6 shows tracking errors of the motor with and without auxiliary control in revolution. It can be seen that the tracking error with auxiliary control is approximately 67% of that without auxiliary control for most of the time. An exception is when the loading object is dropped down to the floor, from which it can be seen that the tracking error with auxiliary control is approximately

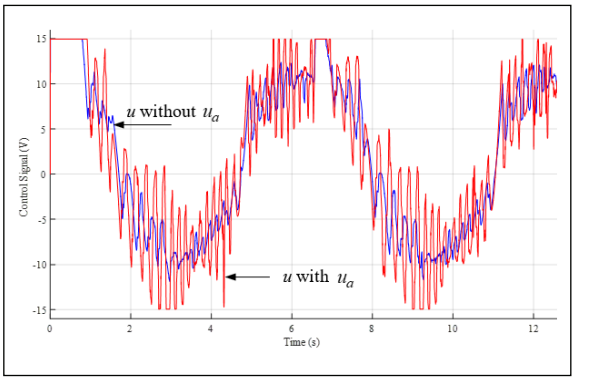

Figure 7: Control Input with and without auxiliary control (unit: V).

the same as that without auxiliary control. The difference in responding speed is insignificant.

Figure 7 shows control input u with and without auxiliary control. Both vary similarly, but the former fluctuates more rapidly and largely than the latter does. For this, the magnitude of fluctuation of the control input u with auxiliary control is approximately 210% of that without auxiliary control. Notice that the amplifier limits the magnitude of control input u to 15 V. The control input reaches the limit briefly in the beginning, and when the loading torque changes abruptly as mentioned above. The same set of experiments is repeated for three rounds, and all the results are found to be very consistent. It may be possible to decrease tracking error significantly by selecting a different performance index for the LQR or by tuning the two design parameters of the auxiliary control, but there is no need to pursue this because the present result is already sufficient to show the benefit of the auxiliary control.

6 Discussions

The proposed auxiliary control has several desirable properties not found in many existing DC motor trajectory control techniques that employ the concept of disturbance observer. These include the properties that it requires no current feedback from motor coils, and its structure is very compact. The control requires an estimate of rotor angular acceleration, which is obtained by feeding motor shaft angular velocity to a low-pass differentiator (LPD). The LPD employed here requires only one positive real design parameter

a_f. This parameter governs its cut-off frequency, which should be slightly higher than the frequency of the load torque. The strength of disturbance compensation is governed by the other positive real design parameter γ. Totally, only two design parameters are to be selected.

Augmenting the proposed auxiliary control to an existing PID control amounts to changing the three PID feedback gains and adding another feedback gain for the output of the above LPD. Because many present-day controllers are programs running on electronic hardware, the auxiliary control can be implemented very conveniently by modifying a few lines of the programs. Neither hardware cost nor hardware size involves in applications of the auxiliary control.

The proposed auxiliary control results from a practical attempt to improve disturbance rejection of the system discussed in Section 5 without modifying electronic hardware. Preliminary experimental investigation on other systems reveals that it could also be particularly useful for disturbance rejection of DC motor trajectory control systems in which significant cogging torque is present. In situations when DC motors are employed to drive objects of varying mass moment of inertia, an adaptive scheme for adjusting the feedback gains to improve disturbance rejection is to be investigated.

7 Conclusions

When an articulated robot arm operates, it is practical that a joint motor is subjected to large loading variations due to gravity. This variation can occur smoothly or abruptly and can increase tracking error significantly. In practice, PID controllers are usually employed as independent joint motor controllers because of numerous successful records and available theoretical results. However, it appears that their ability to handle fast loading variation is often not very satisfactory. This paper proposes a linear auxiliary control that specifically handles such loading variation, and augments conveniently to the existing PID controllers. The auxiliary controller employs the concept of disturbance observer to quickly estimate loading torque, which cannot be measured directly in practice. The auxiliary control does not require feedback from the motor coil current. This makes it particularly useful for robots that do not have such feedback available. DC joint motors are considered here primarily because they are relatively economical, and simple to drive. By augmenting the auxiliary control to the existing PID control, the corresponding linear resultant control is obtained. The system matrix of the resulting linear control system is explicitly given to facilitate direct applications of existing robust stability analysis theorems for linear systems. For the cases in which all the relevant parameters can be regarded as constants, input-to-state stability of the system is guaranteed when the system matrix is strictly Hurwitz. Criteria for assuring this type of stability in practical situations are discussed extensively in the literature and many useful results are readily available. Experiments are conducted to investigate the disturbance rejection capability of the auxiliary control. For this, the auxiliary control is augmented to a PID control obtained by using LQR theory, and the resultant control is applied to a DC joint motor of an articulated robot arm to track a reference trajectory. Along the given reference trajectory, smooth and abrupt loading variations due to gravity are applied to the motor. It appears from the experimental results that the auxiliary control can improve disturbance rejection of the PID control system significantly and consistently.

Acknowledgements

The articulated robot and the associated control system employed in Section 5 belong to the Department of Mechanical Engineering, Rangsit University.

Author's Contributions

All the work in this manuscript is completed by the author. The author has read and agreed to the published version of the manuscript.

Conflicts of Interest

The author declares no conflict of interest.

References

[1] F. Nagata and K. Watanabe, *Controller Design for Industrial Robots and Machine Tools: Applications to Manufacturing Processes*. Wisconsin: Woodhead, 2013, pp. 91–112.

[2] M. Wilson, *Implementation of Robot Systems*.

Amsterdam, Netherlands: Elsevier, 2015, pp. 75–102.
[3] D. G. Caldwell, *Robotics and Automation in the Food Industry*. Wisconsin: Woodhead, 2013, pp. 21–34.
[4] R. N. Jazar, *Theory of Applied Robotics*, 2nd ed., Berlin, Germany: Springer, 2010, pp. 838–842.
[5] C. Fallaha, M. Saad, J. Ghommam, and Y. Kali, "Sliding mode control with model-based switching functions applied on a 7-DOF exoskeleton arm," *IEEE/ASME Transactions on Mechatronics*, vol. 26, no.1, pp. 539–550, Feb. 2021.
[6] X. Yin and L. Pan, "Enhancing trajectory tracking accuracy for industrial robot with robust adaptive control," *Robotics and Computer-Integrated Manufacturing*, vol. 51, pp. 97–102, Jun. 2018.
[7] S. Chen and J. T. Wen, "Industrial robot trajectory tracking control using multi-layer neural networks trained by iterative learning control," *Robotics*, vol. 10, no. 1, Mar. 2021, Art. no. 50.
[8] S. Ling, H. Wang, and P. X. Liu, "Adaptive fuzzy tracking control of flexible-joint robots based on command filtering," *IEEE Transactions on Industrial Electronics*, vol. 67, no. 5, pp. 4046–4055, May. 2020.
[9] K. Ohishi, K. Ohnishi, and K. Miyachi, "Torque – speed regulation of DC motor based on load torque estimation method," in *International Power Electronics Conference*, 1983, pp. 1209–1218.
[10] S. Emre, O. Roberto, and O. Kouhei, "Disturbance observer-based robust control and its applications: 35th anniversary overview," *IEEE Transactions on Industrial Electronics*, vol. 67, no. 3, pp. 2042–2053, Mar. 2020.
[11] S. Emre and O. Kouhei, "Stability and robustness of disturbance observer based motion control systems," *IEEE Transactions on Industrial Electronics*, vol. 62, no. 1, pp. 414–422, Jan. 2015.
[12] R. Carlson, M. Lajoie-Mazenc, and J. C. d. S. Fagundes, "Analysis of torque ripple due to phase commutation in brushless DC machines," *IEEE Transactions on Industry Applications*, vol. 28, no. 3, pp. 632–638, May 1992.
[13] Ramin S. Esfandiari, and B. Lu, *Modeling and Analysis of Dynamic Systems*, 3rd ed., Florida: CRC Press, 2018, pp. 295–296.
[14] H. K. Khalil, *Nonlinear Systems*, 3rd ed., New Jersey: Prentice Hall, 2002, pp. 346–350.
[15] S. P. Bhattacharyya, A. Datta, and L. H. Keel, *Linear Control Theory: Structure, Robustness, and Optimization*. Florida: CRC Press, 2009.
[16] R. K. Yedavalli, *Robust Control of Uncertain Dynamic Systems*. Berlin, Germany: Springer, 2014, pp. 47–59.
[17] G.-R. Duan, and H.-H. Yu, *LMIs in Control Systems*. Florida: CRC Press, 2013, pp. 110–119.